Available online at www.sciencedirect.com
SCIENCE DIRECT
International Journal of Heat and Mass Transfer 49 (2006) 2931–2938
International Journal of HEAT and MASS TRANSFER
www.elsevier.com/locate/ijhmt

Mass transfer coefficients associated with the mixing of a confined gas volume by the random motion of loose spheres

Herek L. Clack *, Aamer A. Mohammed

Department of Mechanical, Materials and Aerospace Engineering, Illinois Institute of Technology, 10 West 32nd Street, Chicago, IL 60616, USA

Received 14 February 2005; received in revised form 8 February 2006
Available online 24 April 2006

Abstract

This investigation quantifies the change in mass transfer within a confined gas volume subjected to mixing by loose spheres. A cylindrical vessel containing between 1 and 50 Teflon spheres in a tracer gas is vigorously shaken. Extractive sampling provides time histories of tracer gas concentrations extracted from the vessel. Fitting the results from a simple 1-D mass transfer model to the experimental data yields an effective mass transfer coefficient k' for each experimental condition. Compared to diffusive mass transfer where $k' = D_{ab} = 7.58 \times 10^{-6}\ \mathrm{m^2/s}$, k' exhibits a cubic dependency on the number of spheres with a maximum at 17 spheres where $k' = 3.5 \times 10^{-3}\ \mathrm{m^2/s}$.

1. Introduction

Aerosols used in industrial processes have a number of characteristics that complicate their study as compared to the study of atmospheric aerosols. Short characteristic time scales, intense turbulence, and often-rapid surface reactions confound both acquisition of experimental data and numerical modeling. Of particular interest recently are particle-laden jets used to inject powdered sorbent. Such jets are widely used in technologies developed to control the emission of trace metals such as mercury from combustion processes [1–3]. Because the combustion exhaust is initially sorbent-free, and the sorbent-laden jet is initially mercury-free, jet phenomena such as jet spreading, entrainment, and turbulent mixing arise as important factors governing the efficient uptake of the targeted pollutant.

The study of jet phenomena is common in fluid dynamics, both for pure (single-phase) gas jets in both quiescent and co-flowing media [4–9] and for particle-laden jets [10–13]. However, most such studies have sought further insight into phenomena purely of a fluid dynamic nature. Our recent research [14] has sought to provide insight on the coupling between fluid mechanics of particle-laden jets and interphase mass transfer and adsorption often referred to as *entrained flow* or *in-flight adsorption*. The present experimental apparatus, an aerosol chamber, was developed to study the adsorption of trace gases by suspended powdered sorbent material under varying thermofluid conditions (e.g., temperature, relative humidity). In addition, turbulent mixing of the suspensions is possible by vigorously agitating the chamber while it contains varying numbers of loose spheres. The objective of the present investigation is to quantify this turbulent mixing in terms of an effective mass transfer coefficient k'. The approach involves filling the chamber with a known concentration of a tracer gas and recording its elution from the chamber over time under different turbulent mixing conditions. Calibrating a simple 1-D mass transfer model to the experimental results yields a value of k' in the chamber based on the evolution of the toluene concentration distribution along the chamber axis. This effective mass transfer coefficient is analogous to the turbulent eddy diffusivity, ε_T, the scalar coefficient that relates concentration gradient and mass flux for turbulent flows.

* Corresponding author. Tel.: +1 312 567 3184; fax: +1 312 567 7230.
E-mail address: clack@iit.edu (H.L. Clack).

0017-9310/$ - see front matter © 2006 Elsevier Ltd. All rights reserved.
doi:10.1016/j.ijheatmasstransfer.2006.02.014

Nomenclature

A	cross sectional area
C	molar concentration
D	diameter, aerosol chamber
d	diameter, branch arm, sampling gas fitting
D_{ab}	molecular diffusion coefficient
h_m	convective mass transfer coefficient
k'	effective mass transfer coefficient
L	length of the aerosol chamber
$\dot{m}$	mass flow rate
P	pressure
ppmv	part per million concentration, by volume
Q	volumetric flow rate
slpm	standard liters per minute
T	temperature
t	time
U	velocity
V	volume
x	axial dimension
y	normal dimension

Greek symbols

α	included angle of oscillation
δ	boundary layer thickness
ε_T	turbulent eddy diffusivity
ϕ	azimuthal angle, in spherical coordinates
μ	dynamic viscosity
ρ	mass density
ν	kinematic viscosity, μ/ρ
ω	frequency

Subscripts

chamber	aerosol chamber
cr	critical value
Fitting	sampling gas fitting
i	inboard end, branch arm, tee fitting
in	gas inlet, White cell
ive	interfacial volume element
o	outboard end, branch arm, tee fitting
out	gas outlet, White cell
0	baseline

2. Experimental method

Fig. 1 presents a schematic of the overall experimental method in which the time-dependent concentration of a trace gas (toluene) within an aluminum aerosol chamber is extractively measured by Fourier transform infrared (FTIR) spectroscopy under different mixing conditions, those conditions resulting from the physical agitation of the chamber itself. The aerosol chamber is a cylindrical aluminum vessel with interior dimensions of 16.4 cm length and 13.7 cm diameter providing an interior volume of 2.09 L (Fig. 1, left). O-rings fitted to the two circular endplates maintain an airtight seal. The endplates are fitted with gas fittings for pressurizing or evacuating the chamber. Mounted at the center of one end plate is a 3/4″ tee fitting (1.5 cm diameter, 2.7 cm length) used for extractive sampling from the chamber. The sampling method resembles the operation of a Stefan tube, a capillary tube open at one end, closed at the other end which holds a volatile liquid. When a gas flow of constant velocity is directed over the open end of the tube, the mass transfer of vapor from the liquid surface to the gas stream produces a predictable decrease in the liquid level in the tube. In the sampling method described here, the aerosol chamber replaces the volatile liquid. The tee fitting connects the aerosol chamber to the gas-sampling stream and serves as the head of the sampling train (Fig. 1, left). The branch arm of the tee fitting connects directly to the aerosol chamber. One of the two run arms connects to an 8.5 L multi-pass White cell (Infrared Analysis, Anaheim, California) through 2.35 m of 1/4″ Teflon tubing. The other run arm is open to the laboratory environment. A vacuum pump downstream of the White cell induces the gas sampling flow and a rotometer maintains a constant flow rate (21.9 slpm) through the sampling train.

The present investigation examines turbulent mixing in the chamber involving 0, 1, 10, 25, and 50 quarter-inch (0.635 cm) diameter Teflon spheres. After adding the desired number of spheres, the 2.09-L chamber is charged with 0.4 L of a dilute (35,150 ppmv) toluene ($C_5H_5CH_3$)/nitrogen (N_2) gas mixture at a rate of 1.17 slpm. A stream of nitrogen gas, bubbled through a constant-temperature liquid toluene bath, provides the gas mixture. A rotometer maintains a constant nitrogen gas flow rate, which along with the constant bath temperature, has been found to provide a constant toluene concentration in the gas stream. Toluene is a common sorbate whose adsorption isotherms are readily available. Commonality between the present investigation and future in-flight adsorption experiments was the primary consideration in its selection. A second valve at the opposite end of the chamber remains open during the charging process to maintain atmospheric pressure within the chamber. After charging, the valves are closed and the gas mixture rests for 10 min to promote a more axisymmetric toluene concentration distribution in the chamber. Preliminary results (not shown) revealed that a 10-min

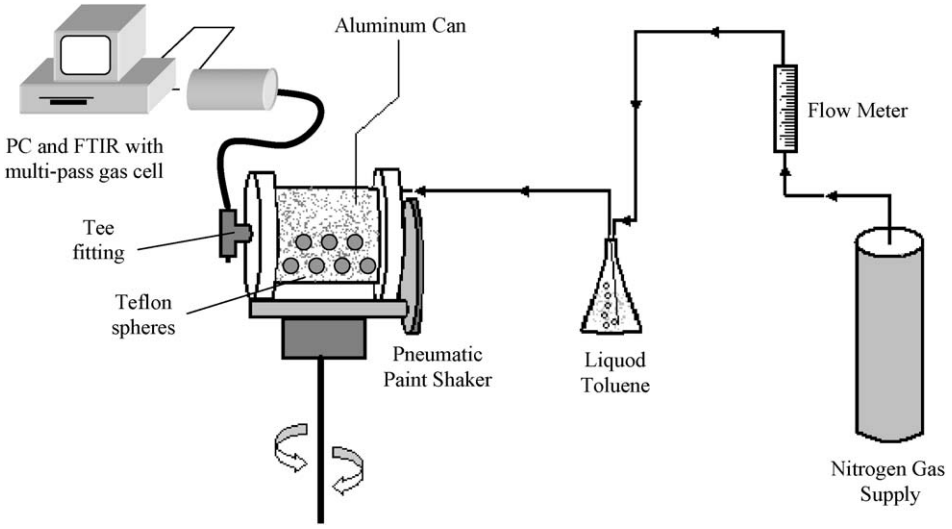

Fig. 1. Schematic of experimental setup (not drawn to scale).

delay after charging produced the same experimental results as 20- and 30-min delay periods. Gas sampling starts simultaneously with the agitation of the chamber by a pneumatic paint shaker.

The White cell is optically connected to a Fourier transform infrared (FTIR) spectrometer (Thermonicolet, Madison, Wisconsin). The FTIR spectrometer acquires absorbance spectra for gas mixtures in the wave number range of about 550–4000 cm^{-1} at an operator-selected scan rate of approximately 1 Hz. A subtraction method using the toluene spectral feature centered at 3041 cm^{-1} was used to quantify the toluene concentration associated with each collected IR spectrum. Each experimentally obtained concentration measurement reflects an average of 32 spectral scans. The time required for spectral averaging (≈30 s) and the ventilation time scale of the White cell (≈23 s) mean that measured toluene concentrations represent an approximately 30 second rolling average. Total gas sampling time at each experimental condition is typically 1500–2000 s. The White cell provides a 16.8 m IR absorption path length, enabling measurement sensitivities of less than 1 part per million. Such precision constitutes an improvement over earlier generations of mass transfer experiments whose precision was often no better than +/−30% (+/−300,000 ppmv) [15].

3. Numerical method

One shortcoming of extractive sampling is that the experimental data represent toluene concentrations in the White cell, not toluene concentrations within the chamber. Thus, to allow comparison between the model and the experimental data, the numerical model encompasses the aerosol chamber, the tee fitting, and the White cell, three interconnected control volumes designed to represent as faithfully as possible the actual experimental configuration. The model does not account for the 2.35 m of tubing between the tee fitting and the White cell because gas residence times there are short (70 ms) and the tubing is impermeable. Globally, with the exception of the binary mass diffusivity for toluene into air D_{ab}, the model approximates the transport properties of the gas mixture in each control volume as being those of air, an ideal gas, at 292 K. This approximation is reasonable because the gas composition everywhere in the experimental apparatus is that of air containing varying, highly dilute amounts of the toluene/nitrogen mixture. The model is a finite difference algorithm using a time step of 0.1 s. Toluene is assumed inert relative to the aluminum, quartz, and Teflon materials of the apparatus.

3.1. Aerosol chamber

Although the charging process is gradual, toluene concentration distributions in the chamber during and immediately afterwards are likely to be 2-D. The largest gradients are likely to be in the axial and radial directions, with lesser gradients circumferentially because the location of the injection port on the cylindrical chamber axis provides axisymmetry. Despite the diffusion and dispersion of toluene that occurs during and after charging, both axial and radial gradients may persist after the 10-min delay period. Thus, the 1-D mass transfer model is a more accurate representation of mass transfer along the chamber centerline, where radial gradients are negligible and mass transport most closely resembles 1-D behavior. Fig. 2 (left) illustrates the 1-D discretization used in the aerosol chamber and attached tee fitting.

Both the tee fitting and the White cell are not spatially resolved but treated as single volume elements in the model, the rationales and details of which are presented in subsequent sections. For a constant gas-sampling rate, the elution rate of toluene from the chamber determines the toluene concentrations in the sampling gas stream

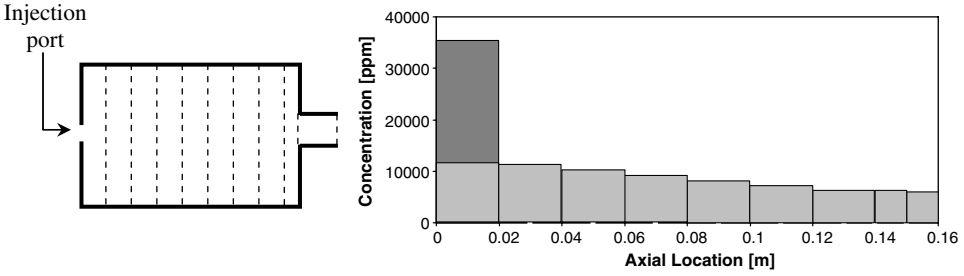

Fig. 2. Schematic of aerosol chamber discretization (left, not drawn to scale), and numerical model values of toluene concentration in the chamber at $t = 0$ (dark gray) and $t = 10$ min (light gray) after charging.

and the White cell as a function of time. The elution rate of toluene from the chamber depends on the mass transfer mechanisms within both the chamber itself and the branch arm of the tee fitting (Fig. 2, left). Once the mass transfer resistance in the branch arm is determined, measured toluene concentrations in the White cell can be directly related to mass transfer within the chamber. The 1-D mass transfer model relates toluene concentrations in the White cell to an effective mass transfer coefficient k' in the chamber.

In discretizing the aerosol chamber, each differential cylindrical element has the same diameter as the chamber and a width of 2 cm, with the exception of the region near the sampling port (Fig. 2, left). The differential element adjacent to the tee fitting has a width of 1 cm for reasons detailed later in this section. The 1-D form of the diffusion Eq. (1) governs mass transfer between these elements.

$$\frac{1}{k'}\frac{\partial C}{\partial t} = \frac{\partial^2 C}{\partial x^2} \tag{1}$$

In (1), under pure diffusive conditions, $k' = D_{ab}$, the molecular diffusion coefficient, calculated using the FSG correlation (2) provided by Fuller and co-workers [16]:

$$D_{ab} = \frac{1.0 \times 10^{-9} T^{1.75}}{P\left[\left({}_a\sum \upsilon_i\right)^{1/3} + \left({}_b\sum \upsilon_i\right)^{1/3}\right]^2}\left(\frac{1}{M_a} + \frac{1}{M_b}\right)^{1/2} \tag{2}$$

in which P is pressure (atmospheres), T is temperature (K), ${}_x\sum \upsilon_i$ represents the sum over all diffusion volumes i in species x, and MW_x is molecular weight of species x (g/g mol). Values for collision integrals for a large selection of molecules are readily available in tabular form (e.g., [15]). The value of D_{ab} determined from (2) for the present analysis is $D_{ab} = 7.58 \times 10^{-6}$ m^2/s for the toluene–air system.

Section 2 describes the partial charging of the chamber with toluene, followed by a 10-min delay to allow the contents to settle. The numerical model simulates the charging as a plug flow, followed by a 10-min period of diffusion between the charged volume (0.4 L, 35,150 ppmv of toluene in nitrogen) and the remaining gas in the chamber (1.69 L of air). Fig. 2 (right) illustrates the toluene concentration distributions in the model before and after the 10-min diffusion period, the latter serving as the initial condition for the model at the start of agitation.

3.2. Interfacial region

Qualitatively, the agitation of the cylindrical aerosol chamber is analogous to the problem of the boundary layer generated in a viscous fluid above a planar solid boundary undergoing periodic in-plane motion (Fig. 3, left). First addressed by Stokes [17], the solution is a function of the viscosity of the fluid and the periodic in-plane motion of the solid boundary (Fig. 3, left). Using the method of separation of variables with appropriate boundary conditions, the analytical solution obtained by Stokes is (3):

$$U(y,t) = U_0 \exp\left(-\sqrt{\frac{\omega}{2\nu}}y\right)\cos\left(\omega t - \sqrt{\frac{\omega}{2\nu}}y\right) \tag{3}$$

where y is the normal distance from the solid boundary (m), ω is the frequency of oscillation (s^{-1}), U_0 is the amplitude of oscillation (m/s), and ν is the kinematic viscosity of the fluid (m^2/s). The form (3) of the solution for $U(y,t)$ reveals the periodic nature of the velocity profile in the viscous boundary layer. The kinematic viscosity, oscillation frequency, and the distance from the oscillating boundary combine in an exponential decay prefactor, causing the amplitude of the velocity in the boundary layer to decrease with increasing y and ω. The result is that for any given oscillation frequency ω, there is a critical distance y_{cr} beyond which the fluid velocity is vanishingly small, constituting a *quiescent region*. For example, for water (at STP) subjected to a periodic velocity boundary condition at a frequency of 10 Hz, the critical distance y_{cr} is 0.8 mm.

Fig. 3 (right) illustrates the phenomenological extension of the Stokes problem we propose to apply to the agitation of the chamber. This phenomenological construction has

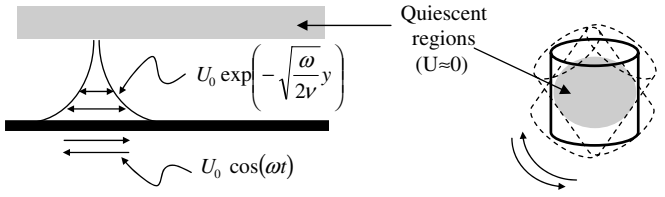

Fig. 3. Schematics of Stokes' oscillating viscous boundary layer flow (left) and the analogous phenomenon for the present investigation (right) (drawings not to scale).

several implications for the mass transfer within the aerosol chamber during agitation, described below. It should be noted that an exact solution for the periodic viscous boundary layer within the chamber is neither sought nor required to complete the 1-D mass transfer model of the chamber.

The internal flow induced by the motion of the aerosol chamber is confined to a viscous boundary layer having a *nominal* thickness $\delta(\omega, v)$ equal to the critical distance $y_{cr}(\omega, v)$ from the chamber walls. A nominal rather than an absolute viscous boundary layer thickness is specified because, unlike the boundary layer in the Stokes problem, the periodic viscous boundary layer generated in the aerosol chamber is not of uniform thickness. To illustrate this point, consider a hollow spherical shell similarly agitated about its polar axis. The periodic motion of the spherical shell imposes on the fluid inside a periodic velocity boundary condition whose amplitude U_0 is a function of latitude (i.e., azimuthal angle ϕ) on the sphere, attaining a maximum value near the equator and tending to zero near the poles of the sphere. Because the amplitude of the periodic velocity boundary condition U_0 varies with ϕ, so too does the induced periodic velocity boundary layer profile (i.e., $U = U(y, t, \omega, v, \phi)$. Thus, defining δ based on a minimum velocity $U(y)$, or minimum velocity differential $(U_0 - U(y))$ as we have done here, leads to $\delta = \delta(\omega, v, \phi)$, with δ decreasing with decreasing ϕ. Although the present aerosol chamber is cylindrical, its circular cross section traces out a spherical volume when the chamber rotates about any axis other than its longitudinal axis (Fig. 3, right). The relatively small aspect ratio of the cylinder ($L/D = 1.3$) tends to maximize this spherical body of revolution relative to the cylinder volume.

The behavior of this viscous boundary layer is important because it mediates mass transfer between the quiescent core region of the chamber ($y > \delta, U = 0$) and the tee fitting. During purely diffusive conditions in the chamber (no agitation), extractive sampling of toluene creates concentration gradients in the immediate vicinity of the tee fitting. During agitation, this region falls within the periodic viscous boundary layer and is subjected to viscous shear and complete flow reversal every cycle (every $1/\omega$ s). Such vigorous mixing is likely sufficient to maintain a ''well-mixed'', spatially uniform concentration throughout the viscous boundary layer. Consequently, in the numerical model this region has a time-varying but spatially uniform concentration throughout. This well-mixed assumption only applies to the region of the chamber subject to the periodic viscous boundary layer, which only occurs during agitation. The discretization in the chamber near the tee fitting (Fig. 2, left) is scaled to match the calculated periodic viscous boundary layer thickness δ, so that its effects are confined to a single differential volume element called the *interfacial volume element*. The value of δ ($\sim$1 cm) is calculated from (3), setting U_0 equal to the rotational velocity of the endplates during agitation ($\alpha\omega L/2$), where α is the included angle of agitation (45°) and $L/2$ is the radius of gyration. Because the included angle of agitation is relatively small, the numerical model neglects centripetal effects.

The presence or absence of agitation implies different boundary conditions (convective or diffusive, respectively) between the interfacial volume element and the tee fitting. Thus, the mass balance equation that yields the rate of change of toluene concentration for the interfacial volume element dC_{ive}/dt differs by one term for conditions without (4) and with (5) agitation:

$$\text{Without agitation: } \frac{dC_{ive}}{dt} = k'\left(-\frac{A_{chamber}}{V_{ive}}\frac{dC}{dx}\bigg|_{chamber} + \frac{A_{fitting}}{V_{ive}}\frac{dC}{dx}\bigg|_{fitting}\right) \quad (4)$$

$$\text{With agitation: } \frac{dC_{ive}}{dt} = -k'\frac{A_{chamber}}{V_{ive}}\frac{dC}{dx}\bigg|_{chamber} - h_{m,i}\frac{A_{fitting}}{V_{ive}}(C_{ive} - C_{fitting}) \quad (5)$$

where V_{ive} is the volume of the interfacial element, k' is the effective mass transfer coefficient ($=D_{ab}$ under purely diffusive conditions), $h_{m,i}$ is the convective mass transfer coefficient at the inboard end of the branch arm of the tee fitting, and A_x and C_x are the cross sectional area for mass transfer and concentration in region x, respectively.

Under purely diffusive conditions (without agitation), the cross sectional area of the interfacial volume element equals that of the chamber ($A_{chamber} = \pi R^2$ in Fig. 2, left). It is clear, however, that this value does not hold during agitation. Because the endplate and embedded tee fitting rotate in an arc around the stationary quiescent core, the interfacial area for mass transfer between the two regions also traces an arced path. The time-averaged effect during agitation is a larger interfacial area for the interfacial volume element in (5), with $A_{chamber} = \pi R^2 + 2R(\alpha L/2)$. The additional term represents the additional area swept by the endplate during agitation, where α is the included angle of agitation (45°) and $L/2$ is the radius of gyration.

3.3. Tee fitting

The inboard end of the branch arm of the tee fitting passes through the center of one of the end plates and connects to the chamber. The outboard end connects to the gas sampling line (Fig. 1), transferring toluene from the chamber to the gas sampling line in a manner similar to a Stefan tube. Unlike a Stefan tube, however, preliminary numerical results revealed that a Fickian diffusion model underpredicts mass transfer through this section. A review of the literature suggests that conditions in the branch arm of the tee fitting are conducive to lid-driven cavity flow. Prasad and Koseff [18] and Koseff and Street [19,20] investigated lid-driven cavity flows at Reynolds numbers Re_D as low as 1000. In the present investigation, the cross flow within the tee fitting results in a far higher Reynolds number ($Re_D = 30{,}200$). Lid-driven cavity flow induces a continuous, volumetric circulation that would maintain convective boundary conditions at both ends of, and a well-mixed uniform concentration throughout, the branch arm of the tee fitting.

Because the lid-driven cavity flow is induced by the continuous sampling gas flow, the resulting convective boundary conditions within the branch arm exist under all experimental conditions. In addition, during agitation, the periodic viscous boundary layer in the interfacial volume element enhances convective mass transfer between the chamber and the branch arm. Thus, the convective boundary conditions at the outboard and inboard ends of the branch arm of the tee fitting are single- and double-valued, respectively, in the model. The convective mass transfer coefficient at the outboard end, $h_{m,o}$, has a constant value, while the corresponding coefficient at the inboard end, $h_{m,i}$, takes on different values with and without agitation. Under all conditions, the time-varying, spatially uniform concentration in the well-mixed branch arm of the tee fitting is governed by a mass balance Eq. (6):

$$\frac{dC_{fitting}}{dt} = \frac{1}{L}(h_{m,i}(C_{ive} - C_{fitting}) - h_{m,o}(C_{fitting} - 0)) \quad (6)$$

where L is the length of the fitting ($=V_{fitting}/A_{fitting} =$ 2.7 cm), $h_{m,i}$ and $h_{m,o}$ are the inboard and outboard convective mass transfer coefficients, respectively, and $C_{fitting}$ and C_{ive} are the concentrations in the tee fitting and the interfacial volume element, respectively. The sampling gas stream adjacent to the outboard end of the branch arm is free of toluene. The constant outboard convective mass transfer coefficient ($h_{m,o} = 2.5 \times 10^{-1}$ m/s) is determined by calibrating the model with the experimental data under purely diffusive conditions (no agitation). With $h_{m,o}$ established, the two values of $h_{m,i}$ were similarly determined with ($h_{m,i} = 5.5 \times 10^{-2}$ m/s) and without ($h_{m,i} = 1.5 \times 10^{-2}$ m/s) agitation, the former condition involving no spheres.

3.4. Multi-pass White cell

As discussed in Section 2, the spectrometer and White cell both impact measured toluene concentrations. As configured, the spectrometer requires approximately 30 s to obtain an IR spectrum of the gas mixture in the White cell. Because the characteristic ventilation time of the White cell (23 s based on 8.5 L and 21.9 slpm) is of the same order as the spectral acquisition time, rapidly changing toluene concentrations are not well resolved.

In the numerical model, a plug flow of 2.9 cm/s is assumed through the White cell based on the gas sampling rate and cross sectional area of the cell (21.9 slpm and 0.0127 m^2, respectively). A toluene mass balance on the White cell yields the rate of change of toluene concentration (7):

$$\frac{\partial C}{\partial t} = \frac{Q}{V}(C_{in} - C_{out}) \quad (7)$$

where C is toluene concentration in the White cell (ppmv), C_{in} and C_{out} are the toluene concentrations at the inlet and outlet of the White cell, respectively (ppmv), Q is the gas sampling flow rate (m^3/s), and V is the volume of the White cell (0.0085 m^3). The plug flow assumption produces a 23 s lag in the model between C_{in} and C_{out} ($C_{out}(t) = C_{in}(t - 23)$). For $t < 23$ s, the initial contents of the White cell are expelled and C_{out} is identically zero.

Summarizing, the agitation of the chamber alone produces two distinct fluid regions internally, a quiescent core and a viscous boundary layer of nominal thickness $\delta = \delta(\omega, \nu)$ and nominal periodic velocity profile $U = U(y, t, \omega, \nu)$. Characterized by fluid shear and periodic flow reversal, the viscous boundary layer is well-mixed throughout and encircles the quiescent core region. Without Teflon spheres, mass transfer within the quiescent core region of the chamber occurs by molecular diffusion, modeled here by (1), where the effective mass transfer coefficient k' is set equal to D_{ab} for the toluene–air system ($D_{ab} = 7.58 \times 10^{-6}$ m^2/s, obtained from (2)). With one or more Teflon spheres added to the chamber, their random motion during agitation increases mass transfer within the quiescent core. This increase in mass transfer is modeled by increasing the value of k' until the model results replicate the experimental data.

4. Results and discussion

Fig. 4 presents the temporal evolution of toluene concentration during agitation with 0, 1, 10, 25, and 50 spheres, both experimental data (symbols) and numerical modeling results (lines). Each numerical modeling result is presented with the relevant value of k' used in the model. The numerical modeling results represent the best fit to the companion experimental data at each experimental condition.

The lowest measured toluene concentrations (Fig. 4) correspond to purely diffusive conditions (no agitation) and were used to calibrate $h_{m,i}$ and $h_{m,o}$. These experimental data show a broad peak in concentration near 150 s, followed by a gradual decay. The numerical model provides

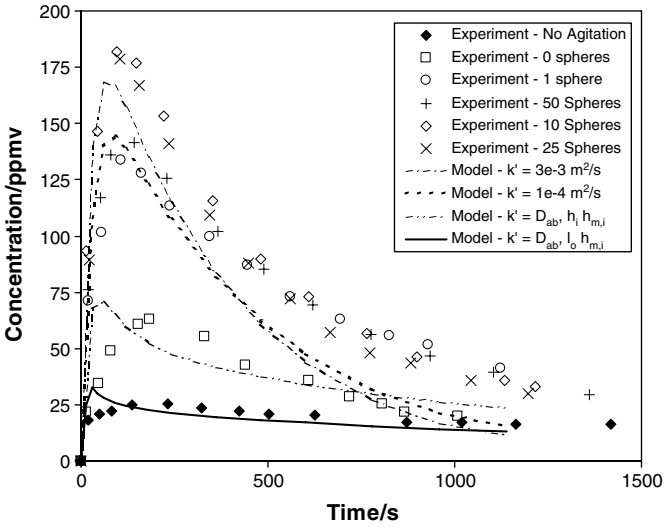

Fig. 4. Temporal evolution of toluene concentration, comparison between experimental and numerical modeling results. Effective mass transfer coefficient values k' noted for each numerical result.

an excellent fit to the experimental data at longer times using $k' = D_{ab} = 7.58 \times 10^{-6}$ m^2/s as calculated from (2). The model, however, predicts an earlier, more pronounced peak concentration than the experimental data. Such differences are consistent with the previously discussed difficulties presented by the White cell and spectrometer when measuring rapid transients. It should be reiterated that the sampling gas stream traverses the 2.35 m of tubing not included in the numerical model in 70 ms, a negligible delay that is not likely to explain the difference between the predicted and measured peak concentration times.

Of significant interest are the experimental results reflecting agitation of the empty chamber in Fig. 4 (legend: $k' = D_{ab}$, *hi* $h_{m,i}$). Compared to the pure diffusion data without agitation (Fig. 4, legend: $k' = D_{ab}$, *lo* $h_{m,i}$), the effect of agitation is to significantly increase the peak concentration. The measured peak concentration during agitation with no spheres occurs at approximately the same time (~100 s) as for the pure diffusion results, suggesting similar phenomena between the two experimental conditions. The higher toluene concentrations during agitation without spheres reflects the higher value of $h_{m,i}$ associated with the increased mass transfer between the chamber and the tee fitting as a result of the periodic viscous boundary layer. The relative impact of agitation on $h_{m,i}$ is made clearer by considering Sherwood number ($Sh \equiv h_m d/D_{ab}$) for the two values of $h_{m,i}$. In the absence of agitation, $h_{m,i} = 1.5 \times 10^{-2}$ m/s and $Sh = h_{m,i} d/D_{ab} = 30$. Such a large Sherwood number indicates that convective mass transport far exceeds diffusive mass transport between the tee fitting and the interfacial volume element. Prominent concentration gradients would be expected in the interfacial volume element near the fitting, and the rate of diffusive transport through this region ultimately limits the measured toluene concentrations. With agitation, however, the mixing within the interfacial volume element eliminates such gradients, thereby increasing the measured toluene concentrations. The viscous boundary layer also imposes additional convective conditions, increasing $h_{m,i}$, Sh and the measured toluene concentrations. The numerical results show the same increase in toluene concentration during agitation with no spheres (Fig. 4, legend: $k' = D_{ab}$, *hi* $h_{m,i}$), with the model predicting an earlier peak value than the experimental data. These numerical results represent diffusive conditions within the quiescent core, $k' = D_{ab} = 7.58 \times 10^{-6}$ m^2/s.

The experimental and numerical results for agitation with 1, 10, 25, and 50 spheres show better agreement between their peak values, with the numerical results predicting a more rapid decay in toluene concentration at extended values of t. The different numerical results reflect different values of k' in the chamber, with $h_{m,i}$ and $h_{m,o}$ held constant (5.5×10^{-2} m/s and 2.5×10^{-1} m/s, respectively). Interestingly, the variation of k' with the number of spheres appears to have a maximum, whereby the effective mass transfer coefficient actually decreases with increasing numbers of spheres. This suggests that beyond an optimum

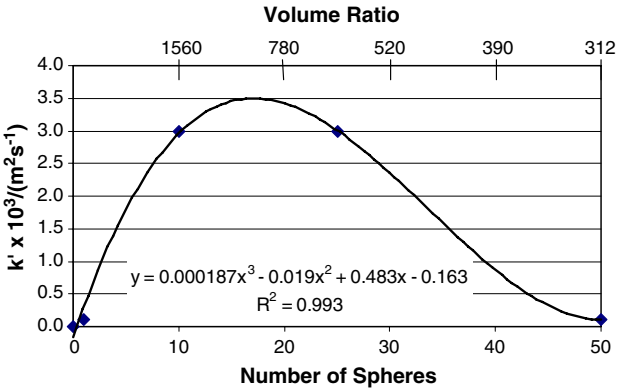

Fig. 5. Variation of effective mass transfer coefficient k' with number of spheres (lower x-axis) and reciprocal of the volume fraction occupied by the spheres (upper x-axis) in the chamber. Cubic curve fit to data shown.

number of spheres (based on the relative size the spheres and the chamber itself), additional spheres have the effect of inhibiting mass transfer. It is clear that as the collective volume of the spheres increases, their motion would be impeded, thereby limiting their potential to enhance mass transfer. However, 50 of these 1/4″ spheres comprise less than 1% of the chamber volume. This implies that only very dilute volume loadings, i.e., collective volume of spheres compared to the mixing volume, are necessary to enhance mass transfer. A cubic curve fit of k' as a function of number of spheres (Fig. 5) reveals an optimum at 17 spheres of $k' = 3.5 \times 10^{-3}$ m^2/s. The reciprocal of the volume fraction occupied by the spheres is plotted as a second, upper x-axis in Fig. 5 to illustrate the dependency of effective mass transfer coefficient with volume loading. It is likely that a different optimum exists for different size spheres, different volume loadings, and perhaps for different sphere mass densities.

5. Conclusions

Experimental data reveal how loose spheres moving randomly influence mass transfer within a closed volume. Concentrations of a trace gas drawn from a vigorously agitated cylindrical vessel are measured by extractive Fourier transform infrared spectroscopy. Using a 1-D numerical model to validate the experimental results, the temporal evolution of toluene concentrations can be interpreted relative to the mixing conditions within the vessel. Purely diffusive results (no agitation) demonstrate good agreement between the experiment and the numerical model. During agitation without spheres, a periodic viscous boundary layer forms adjacent to the vessel walls, enhancing mass transfer from the vessel. Surrounded by this boundary layer is a smaller, quiescent spherical volume in which bulk velocity is vanishingly small. During agitation with from 1 to 50 loose Teflon spheres, each condition is correlated to an effective mass transfer coefficient k' that relates mass flux in the vessel to local concentration gradient. A maximum value of $k' = 3.5 \times 10^{-3}$ m^2/s is inferred from the

experimental and numerical results, associated with the mixing induced by 17 quarter-inch spheres. Both experimental data and numerical results indicate that beyond this maximum, greater numbers of spheres have the effect of inhibiting mass transfer within the vessel. On a volume fraction basis, the maximum value of k' associated with 17 spheres represents a very dilute volume loading of less than 1% of the volume of the vessel.

References

[1] S.D. Serre, B.K. Gullett, S.B. Ghorishi, Entrained-flow adsorption of mercury using activated carbon, J. Air Waste Manage. Assoc. (51) (2001) 733–741.

[2] Public Service Company of Colorado/ADA Technologies, Inc., Investigation and Demonstration of Dry Carbon-Based Injection for Mercury Control; Final Report Under Phase I DOE/FETC Mega PRDA Program (period of performance September 1995–July 1997), 1997.

[3] M.V. Scotto, M. Uberoi, T.W. Peterson, F. Shadman, J.O.L. Wendt, Metal capture by sorbents in combustion processes, Fuel Process. Technol. (39) (1994) 357–372.

[4] F.P. Ricou, D.B. Spalding, Measurements of entrainment by axisymmetrical turbulent jets, J. Fluid Mech. (11) (1961) 21–33.

[5] R.A. Antonia, R.W. Bilger, An experimental investigation of an axisymmetric jet in a co-flowing air stream, J. Fluid Mech. (61) (1973) 805–822.

[6] T.B. Nickels, A.E. Perry, An experimental and theoretical study of turbulent coflowing jet, J. Fluid Mech. (209) (1996) 157–182.

[7] P.C.K. Chu, J.H. Lee, V.H. Chu, Spreading of turbulent round jet in coflow, J. Hydraulic Eng. 125 (1999) 193–204.

[8] A.M. Falcone, J.C. Cataldo, Entrainment velocity in an axisymmetric turbulent jet, J. Fluids Eng. 125 (2003) 620–627.

[9] D. Han, M.G. Mungal, Direct measurement of entrainment in reacting/nonreacting turbulent jets, Combust. Flame 124 (2001) 370–386.

[10] J. Garcia, A. Crespo, A turbulent model for gas-particle jets, J. Fluids Eng. 122 (2000) 505–509.

[11] R. Balachandar, S.R. Mulpuru, M.H. Ungurian, Transport of dry aerosols in turbulent jets, J. Environ. Eng. 124 (1998) 994–1002.

[12] J.-S. Shuen, A.S.P. Solomon, Q.-F. Zhang, G.M. Faeth, Structure of particle-laden jets: measurements and predictions, AIAA J. 23 (1985) 396–404.

[13] A.S.P. Solomon, J.-S. Shuen, Q.-F. Zhang, G.M. Faeth, Structure of nonevaporating sprays, Part I: initial conditions and mean properties, AIAA J. 23 (1985) 1548–1555.

[14] U. Narasimhan, H.L. Clack, Trace gas adsorption within dilute gas-sorbent suspensions: proof-of-concept study and implications for controlling mercury emissions from coal combustion, Int. J. Multiphase Flows, in review.

[15] A.L. Hines, R.N. Maddox, Mass Transfer: Fundamentals and Applications, Prentice-Hall, New York, 1985.

[16] E.N. Fuller, P.D. Schettler, J.C. Giddings, Ind. Eng. Chem. (58) (1966) 19.

[17] G.G. Stokes, On the effect of the internal friction of fluids on the motion of pendulums, Trans. Cambridge Philos. Soc. (9) (1851) 8.

[18] A.K. Prasad, J.R. Koseff, Reynolds number and end-wall effects on a lid-driven cavity flows, Phys. Fluids A (1) (1989) 208–218.

[19] J.R. Koseff, R.L. Street, The lid-driven cavity flow: a synthesis of qualitative and quantitative observations, J. Fluids Eng. (106) (1984) 390–398.

[20] J.R. Koseff, R.L. Street, Visualization studies of a shear driven three-dimensional recirculating flow, J. Fluids Eng. (106) (1984) 21–29.